



Pavel Pořízka, Pavlína Modlitbová, and Jozef Kaiser

6.1 Introduction

Investigation of biological samples relies on state-of-the-art instrumentation providing high performance namely in terms of sensitivity and spatial resolution. Optical microscopy is often complemented with other techniques to reach a more complex understanding of investigated phenomena. For those purposes, techniques of analytical chemistry are beneficially used to assess the elemental and molecular composition. The persisting trend in the development of instrumentation and methodology drives away from the direct analysis of sample bulk. However, the bulk chemical analysis through wet chemistry brings the main limitation. The necessity of acid digestion of the sample results in the loss of valuable information about the distribution of elemental/molecular content within the sample.

It has been repeatedly proven that individual diseases manifest themselves also in a significant change in the chemical composition of bodily fluids or tissues [1]. Factual localization of the local singularities in chemical composition and its correlation with changes and degradation of cells is necessary. Providing chemical information with a cell-level resolution is a goal of the spectroscopic community that will have a significant impact on the understanding of disease initiation and proliferation throughout the tissue. Thus, the detection of abundance/deficiency of individual elements/molecules is of paramount interest to biologists. Finally, it must be stressed that in this chapter we restrict our interest to biological tissues, namely soft and hard/calcified tissues. Obviously, imaging the distribution of elements within other biological tissues also found numerous applications that are briefly mentioned and reviewed as well.

Lasers have a broad range of use for therapy and diagnostics of biological tissues [2] with extensions to various medical fields (e.g., dentistry, surgery, dermatology)

P. Pořízka (✉) · P. Modlitbová · J. Kaiser
CEITEC Brno University of Technology, Brno, Czech Republic
e-mail: Pavel.Porizka@ceitec.vutbr.cz

[3]. The laser-tissue interaction is a well-investigated phenomenon in individual applications for which the laser parameters (e.g., laser wavelength, pulse energy, and duration) are optimized [4]. For diagnostic purposes, the laser parameters are varied to the point when they induce desired characteristic response from the investigated tissues. Determination of elemental composition within the laser spot region demands increasing the laser irradiance over the ablation threshold to reach breakdown and plasma formation (GW/cm^2). Laser ablation is, thus, used for material sampling and its characterization is done through the optical emission spectroscopy of laser-induced plasma (LIP) radiation. Pulsed ablation of tissues is well-described in classic literature [5] and will be dissected further in the text.

Laser ablation is typically coupled with optical emission spectroscopy or mass spectrometry while qualitative and quantitative elemental analysis of a sample is obtained. The laser ablation inductively coupled plasma optical emission spectroscopy and mass spectrometry (LA-ICP-OES/MS) is the gold standard in terms of imaging and, thus, the main representative among other techniques of the field in analytical spectroscopy. However, laser-induced breakdown spectroscopy (LIBS) proved to be a suitable alternative due to recent advances in instrumentation and methodology.

LIBS has established its position among other techniques due to its supreme sample throughput and related laser pulse repetition rate. Here we consider the repetition rate as the main benefit of LIBS providing a high number of analyses (spectra) per unit time. Moreover, the LIBS analysis takes a fraction of time also with more robust and less complicated instrumentation when compared to LA-ICP-OES/MS. This makes LIBS a suitable candidate for deployment in various applications with a potential for in-situ analysis of plants and even direct analysis during surgery [6, 7].

The implementation of LIBS to the analysis of various biological samples increasingly attracts attention. Moreover, recent advances have led to promising results in medical and clinical applications which have been a rapidly expanding field since the beginning of this decade (see Sect. 6.4). In general, LIBS provides information about organogenic (e.g., C, O, H, N, P) and macro nutrient elements (e.g., Ca, Mg, K, Na) while lacking considerable sensitivity to reach some biologically relevant minor and trace elements (e.g., Zn, Cu). This analytical performance predetermines LIBS as a complementary technique to LA-ICP-MS which in turn excels in the detection of traces. Their joint utilization has already been studied in the case of bio-tissues, e.g., plants [8], hard tissues (animal teeth) [9], and soft tissues (human tumors) [10]. However, LA-ICP-OES/MS techniques are considered to be a reference to LIBS, which is a contrast to their joint use. Despite that paradox, LA-ICP-related publications provide a vital source of inspiration for further development of LIBS instrumentation and methodology [1, 11–15].

In this chapter, we will focus primarily on the elemental analysis of biological samples (soft and hard/calcified tissues) when the mapping of large-scale areas is involved. Hence, we will refer to the elemental mapping of biological sample surface as the so-called *elemental bioimaging* or just *imaging* in a broader sense. Also, LIBS analysis of other biological tissues (namely plants) is briefly discussed with related

literature. The description of LIBS instrumentation and progress in analytical performance is shown together with concepts of bioimaging (including 3D imaging), and novel approaches to correlative imaging. Remarks on the parameters involved in laser-tissue interaction and sample preparation are also given along with a broader discussion. Then, good practices in data processing are listed in terms of sample discrimination and quantification; basic univariate and advanced multivariate (chemometrics and machine learning) algorithms are mentioned. Finally, imaging of animal and human tissues is dissected with the vision to medical/clinical applications. The chapter is concluded with hints of future perspectives and trends in the development of the field of LIBS bioimaging.

This chapter builds on existing results in current scientific literature. Thus, the reader is referred to respective bioimaging chapters in other LIBS reviews [3, 16–19]. Other literature sources related to the fundamentals of LIBS and its broad applications [20–24], laser-tissue interaction [4, 5], and the use of lasers in medical and clinical applications [2] are also recommended for further reading.

6.2 Laser Ablation of Tissues

6.2.1 Laser Parameters Involved in the Ablation of Tissues

In this chapter, we do not intend to describe the mechanisms of laser-tissue interaction and consequent laser ablation in detail. Presented review was collected from LIBS-related literature and summarizes selected results and conclusions. Moreover, the reader is referred to a more extensive description in other publications [2, 4, 5]. If not stated otherwise, those references were primarily used in this section.

Naturally, the quality of laser-tissue interaction is determined by optical properties of involved soft/hard tissue and the parameters of the laser radiation. First, the composition of soft tissues is dominated by water (50–95%), collagen, hemoglobin, and melanin. Second, hard tissues are composed namely from hydroxyapatite (~96%), and water. From the optical point of view, the wavelength-dependent absorption coefficient of listed building materials is the most important parameter [5] as shown in Fig. 6.1 for the case of soft tissues. Refer to [4] for the absorption coefficient of hydroxyapatite (hard tissues). It is presented as the most critical property to sustain an optimal energy deposition and desired tissue ablation.

The absorption coefficient is of interest to LIBS in three ranges (UV, VIS, and IR) which relate the material properties with the laser source used for ablation. A Nd:YAG laser generating ns laser pulses on fundamental and harmonic wavelengths (1064, 532, and 266 nm) is typically used for this task in LIBS. In general, the absorption of listed tissue compounds is the lowest in IR range and rises in the UV (Fig. 6.1). This includes the case of hydroxyapatite which is not shown in this figure. Water, an important component of soft tissues, has a high increase in the absorption coefficient in the UV and IR ranges, which corresponds to fundamental (1064 nm) and fourth harmonic (266 nm) wavelengths of Nd:YAG. Melanin, dominating chromophore in pigmented tissues (e.g., skin), has a high absorption coefficient in

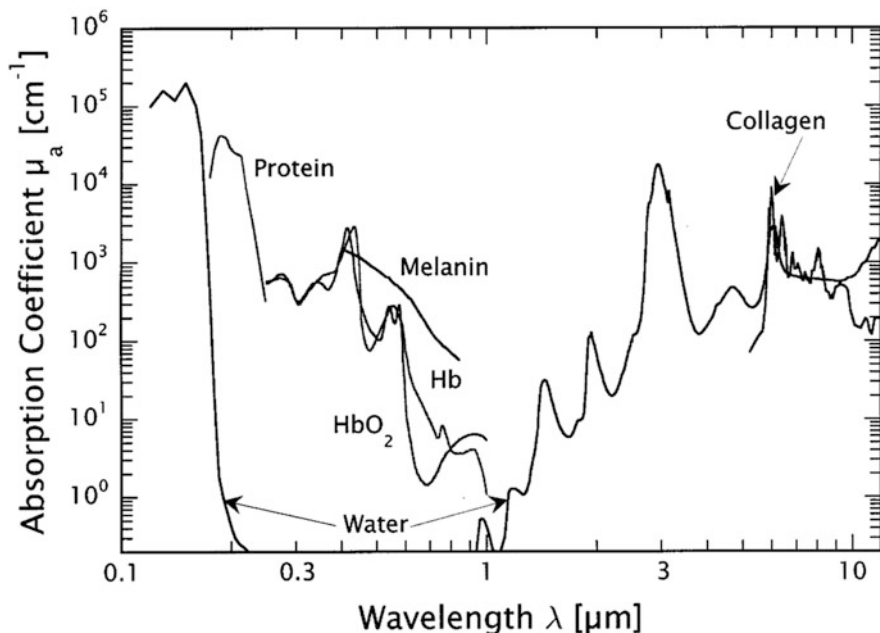


Fig. 6.1 Optical absorption coefficients for selected tissue compounds from 0.1 to 10 μm wavelength range. Hb and HbO₂ correspond to deoxygenated and oxygenated hemoglobin. Obtained from [5] with no permission needed from ACS publications

VIS range where Nd:YAG laser operates on its second harmonic wavelength (532 nm). Thus, the selection of laser wavelength is a crucial step before LIBS analysis.

Harmonics generation is an option to change the wavelength of a pulsed laser, but it is a costly one and it leads to a significant decrease in the peak pulse power. It must be stressed that higher energy is necessary also for the laser ablation with higher harmonics, which is evident when printing relevant irradiances as a function of pulse duration (Fig. 6.2). Selected references with a focus on soft tissues are listed in Table 6.1. Contemporary state-of-the-art LIBS analysis of tissues is dominated by the use of fundamental Nd:YAG wavelength. This is in contrast with the optical absorption coefficients of individual tissue compounds. The fundamental and fourth harmonic wavelengths of an ns-pulsed Nd:YAG laser (1064 vs 266 nm, respectively) were compared in the ablation of murine kidneys [26]. The results of this study pointed toward the advantageous use of 1064 nm for soft tissue ablation as it provided more reproducible ablation and a tighter crater size. The authors suggested that the reason for this was that tissue is transparent to IR radiation, so it is ablated indirectly by the plasma generated on the substrate (150 μm thick cryo sections on a glass slide). Moreover, the increased absorption of the tissue to UV can lead to a broader collateral damage in a broader range. At the same time, the wavelengths of an fs laser (343 and 1030 nm harmonic wavelengths) were selected for the LIBS

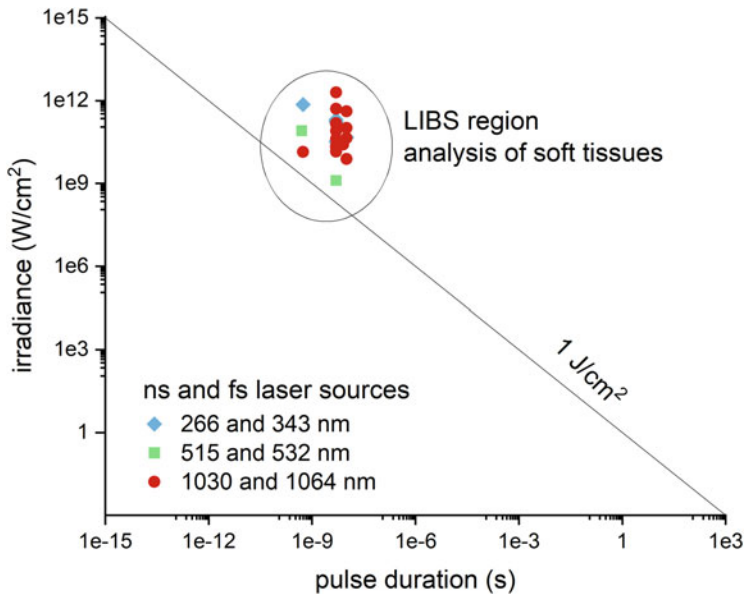


Fig. 6.2 Laser-tissue interaction in terms of pulse duration and irradiance. The circle roughly indicates region of laser-induced plasmas (LIPs) on soft tissues with ns (1064, 532, 266 nm) and fs (1030 and 515 nm) laser sources. Data points were collected from selected literature focused on LIBS analysis of soft tissues. The zoomed region contains references to relevant publications from Table 6.1. Other information on laser-tissue interaction can be found elsewhere [4]

analysis of murine melanoma (40 μm thick sections on a silica substrate) [47]. Their comparison showed similar results as those with the ns-laser ablation—UV wavelength (343 nm) showed higher fluctuations due to inhomogeneity of the tissue and IR wavelength (1030 nm) tended to ablate the tissue indirectly by the ablation of the substrate. The comparison between fs and ns laser pulses is thus appealing for further research while fs lasers are getting more and more affordable and thus are becoming popular in the LIBS community.

Optimization of a LIBS system prior to the analysis is mandatory, however, the optimization of pulse wavelength (UV, VIS, or IR) and pulse duration (fs, ps, and ns) is rare due to complications in the instrumentation. On the other hand, optimization of other experimental parameters (e.g., laser pulse energy, defocus) was discussed in the majority of publications. There is a need for finding the right trade-off between sensitivity and lateral resolution when balancing the amount of ablated material. To achieve the best possible performance, several approaches based on finding the highest signal-to-noise ratio (SNR) were suggested [27, 44]. The optimization in these cases was mostly focusing on the feedback of selected analytes (in the sense of SNR) and the shape and size of the ablation crater. It is advised to implement other optical techniques (e.g., plasma imaging [51] and shadowgraphy [52]) also within the parameter optimization pipeline.

Table 6.1 List of selected publications with focus on the bioimaging of soft tissues or their analysis in the focus. Data assigned with asterisk were not directly given in the referred publication and were estimated from existing information or from similar works of the related research group. Selected publications are ordered from oldest to newest

Sample	Pretreatment	Wavelength (nm)	Duration (ns)	Spot size (μm)	Irradiance (GW/cm^2)	Ref.
Murine kidney	Cryo cutting	1064	5	50	152.9	[25]
Murine kidney	Cryo cutting	1064	5	40	79.6	[26]
Murine kidney	Epoxy resin	266	5	25	32.6	[27]
Murine kidney, tumor	Cryo cutting	1064	5	50	40.8	[28]
Human tumor	Cryo cutting	266	10*	40	171.2	[10]
Murine kidney	Epoxy resin	266	5	10	203.8	[29]
Murine kidney	Epoxy resin	1064	5	30	14.2	[30]
Murine tumor	FFPE	1064	5	50	152.9	[31]
Murine tumor	FFPE	1064	5	30*	141.5	[32]
Murine kidney	Epoxy resin	1064	5	5	509.6	[33]
Skin, lungs, lymph nodes	FFPE	1064	5	66	23.4	[34]
Skin	FFPE	1064	5	50	20.4	[35]
Murine tumor	Cryo cutting	266	10	60	46.7	[36]
Murine kidney, spleen, liver, tumor	Epoxy resin	1064	5	5	509.6	[37]
Cutaneous tumor	Cryo cutting	1030	0.55	65	13.7	[38]
Murine tumor	FFPE	1064	10*	100	7.6	[39]
Murine tumor, cell culture	Cryo cutting	1064	8	25*	25.5	[40]
Brain tumor, cell culture	Cryo cutting	1064	8	25	25.5	[41]
Cells	Freeze-dried	515	0.5	0.5	81.5	[42]
Lung tumor	Cryo cutting	1064	10	45*	408.9	[43]
Murine kidney	FFPE	532	5	100	1.3	[44]
Brain	FFPE	1064	10*	45	44.0	[45]
Cutaneous tumor	FFPE	532	5	100	1.3	[46]
Cutaneous tumor	Cryo cutting	343	0.55	15	720.6	[47]
Lung tumor	FFPE	1064	10*	50	101.9	[48]
Leporine lymph nodes and thyroid glands	Tissue smear	1064	5	22*	1997*	[49]
Brain tumor	FFPE	1064	5	22*	1997*	[50]

6.2.2 Sample Preparation

It is a cliché that there is no need for sample preparation prior to the LIBS analysis of biological tissues. Soft and hard tissues have to be prepared following one or the

other ways reviewed elsewhere [53]. The preparation of hard tissues seems straightforward as the most common approach is epoxy embedding, cutting and fine polishing. The preparation of soft tissues is demanding (consider e.g., the handling of the tissue after biopsy) and two most common approaches used (Table 6.1) are (1) freezing at a cryogenic temperature and (2) formaldehyde fixing and paraffin embedding (FFPE). The latter seems to be more feasible and more convenient for manipulation when enabling the LIBS analysis of cross-sections [44] and direct bulk [46]. The FFPE is the standard procedure in pathology and LIBS has a potential to provide relevant information, but it has to be kept in mind that this kind of sample preprocessing might alter the elemental composition of the tissue and the distribution of elements therein [54].

6.2.3 From the Concept to 3D Bioimaging

The concept of imaging, Fig. 6.3, is a simple application of LIBS when the sample material is ablated from its surface at different positions. In each position, a plasma is generated, and its characteristic radiation is collected by means of optical emission spectroscopy. Obtained spectra are then processed, and estimated intensities of selected spectral lines are printed in images showing the distribution of related elements across the sample surface. Bioimaging approaches are boosted by the advantages of LIBS in general, such as multi-elemental capability, minimal need for sample preparation, high-lateral resolution, and sensitivity. However, those benefits seem contradictory to each other when tuning the experimental settings (e.g., spot size, pulse energy, atmosphere) and optimizing the best possible

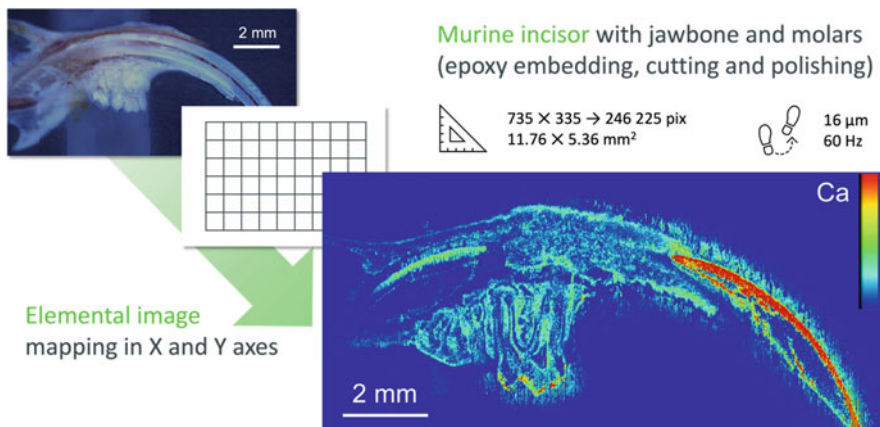


Fig. 6.3 The concept of bioimaging, showing the optical image of epoxy embedded murine incisor (top left), mesh of points in X,Y raster (center), and depicted Ca image (bottom right). The infographics show the total number of pixels and analyzed area, and step size and repetition rate. Authors' unpublished data

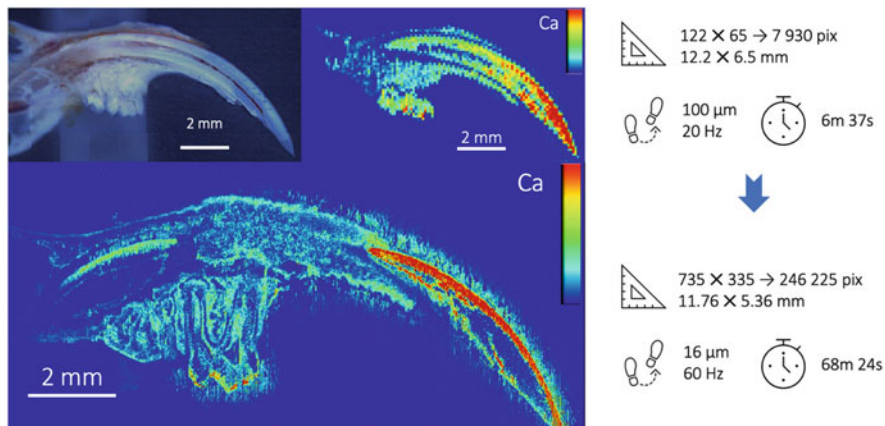


Fig. 6.4 Improvement of the analysis of hard tissues (murine incisor and adjacent jawbone embedded in epoxy resin) in terms of repetition rate and lateral resolution. Authors' unpublished data

performance (e.g., signal to noise ratio, signal to background ratio). Individual issues will be further dissected with respective suggestions.

LIBS imaging is a dynamically evolving field that has recently been driven mainly by the demand from the mining industry [55] and clinical analysis [46]. To give an extreme example of LIBS repetition rate capability, the state-of-the-art instrumentation provides an extreme performance in the analysis of mine drill and cores with 1 kHz repetition rate [56]. Further development of instrumentation for bioimaging will routinely allow elemental imaging with more than 100,000 pixels per sample. For a large-scale sample, the collection of a megapixel image (containing one million spectra) can currently be done within 2 h and 45 min with a 100 Hz laser used. Thanks to this promising performance, LIBS can be used as a fast-prescreening tool in tissue diagnostics before a more precise or sensitive technique is used. However, this tremendous repetition rate yields a high amount of data which requires more intricate data storage and handling (Sect. 6.3.3). The megapixel image will turn into 4.1 GB of data with a simple line CCD detector of a Czerny-Turner (with 2048 pixels per spectrum and 16 bit depth per pixel).

In modern LIBS tissue diagnostics, the desire is the highest possible lateral resolution ($\sim 10 \mu\text{m}$) which reaches the cell level. This spot size leads to the ablation of a low amount of mass and, thus, a low number of emitting species within the LIP. In turn, a higher lateral resolution is usually reached with the decrease in sensitivity and loss of detection capability in the ppm range. This tradeoff is a matter of system optimization. The ablation spot size in the range of 10–30 μm was found as a reasonable tradeoff when yielding satisfactory results even in the ablation of soft [33, 37] and hard tissues [57]. The improvement in lateral resolution over past years, Fig. 6.4, brings more biologically relevant information with finer details in the heterogeneous structure of tissues. To the best of our knowledge, the highest lateral

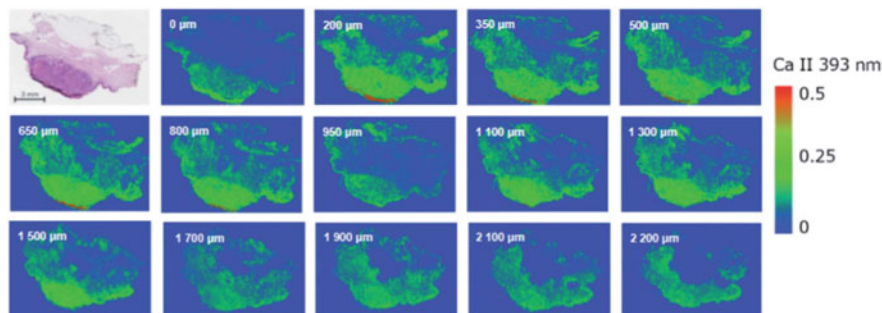


Fig. 6.5 Consequent images of Ca within a bulk of Squamous Cell Carcinoma sample leading to the 3D imaging. The images were obtained by repeated LIBS analysis of consequent sections of paraffine block. The micrometer values refer to the depth from the samples surface (0 μm); the scale shows relative intensity of Ca II 393 nm line. Obtained from [46] while no permission needed from the Royal Society of Chemistry publishing

resolution reached in LIBS bioimaging is on the sub-micron level (~ 500 nm) [42]. In that study, a combination of fs and ns laser pulses (in the orthogonal double-pulse arrangement) was used to image the distribution of InP nanoparticles (NPs) within a single cell (deposited in wells on quartz wafers).

LIBS enables fast analysis of sample surfaces. Then, the whole sample (e.g., model plant) can be ablated in several layers and signal accumulated along the depth reveals “total” (3D) distribution of elements therein [58]. This feature is often used in the so-called 3D imaging where individual layers of the sample surface are consequently ablated. This approach is an extended use of standard depth profiling and gives further information for the sample investigation. The 3D imaging was already demonstrated on the pesticide penetration into the maize leaf [59]. In past years, 3D imaging was used to analyze layers of murine kidney [33], murine brain [45], and even human cutaneous tumor (squamous cell carcinoma) [46] (Fig. 6.5).

6.3 Data Processing

6.3.1 From Qualitative to Quantitative Imaging

In general, LIBS governs multi-elemental capability and enables the detection of organogenic elements (e.g., C, O, H, N, P), macro nutrient elements (e.g., Ca, Mg, K, Na), and potentially trace elements (e.g., Zn, Cu). The detection of endogenous metals (i.e., macro- and micro-nutrient elements) is indispensable for the so-called metallomics, i.e., the detection of relevant metals as biomarkers within the tissue and estimation of the change in their abundance. It was repeatedly confirmed that any disbalance in the endogenous metal content (deficiency or excess) influences the functioning of tissues and may lead to various diseases, including cancer [3, 16, 18]. Moreover, the detection of exogenous metals (i.e., metals artificially

administered to the tissue) also found its place in biological/medical applications (e.g., indirect biomarkers and labels of selected proteins, toxicology).

Many scientific works in the past focused on the analysis of well-selected spots (line scans or small maps) owing to the limitations in the instrumentation performance (repetition rate and incapability of large-scale mapping). However, proper selection of characteristic regions of the investigated sample led to interesting results that paved the way for further LIBS development in imaging. In the beginning, the ablation of hard tissues was more attractive in the LIBS community owing to its more convenient laser-tissue interaction and consecutive ablation. The body of work by Samek et al. showed the potential of LIBS in human teeth analysis; including the pioneering work on the quantification of trace metals [60], matrix-matched calibration of Al, Pb, and Sr [61], and classification of healthy and carious teeth [62]. Later, the group of Kaiser et al. delivered the line scan of Sr and Ba (Ca served as internal standard for both elements) in prehistoric bear tooth [9], LIBS imaging of Ca and P of snake vertebrae complemented X-Ray Computed Tomography (XCT) scan [63], and small-size mapping of Ca and P as age-related changes in the chameleon teeth [64]. Presented publications can be considered as classical LIBS literature. Moreover, further publications showed other significant benefits of LIBS, e.g., in dentistry [65]. The early detection of caries was proved feasible based on the ratio of Zn and Ca content within the tooth [66].

The LIBS-related research in the case of soft tissues is predominantly focused on the diagnostics of cancer [3]. As LIBS generally lacks the detection capability for trace elements, the interest is mainly in the semiquantitative analysis of abundance of major nutrition elements (e.g., Ca, K, Mg, and Na) with trace elements (e.g., Fe, Cu, and Zn) being seldom presented. The changes in elemental composition were found beneficial in the discrimination of healthy and diseased tissues in many cases, e.g., hemangiosarcoma and normal liver [67], breast and colorectal cancers [68], and breast cancer [69]. A similar approach was then used to differentiate cancerous tissues in large-scale imaging (see further in the text). The next step in the data analysis is the implementation of chemometric algorithms and machine learning (Sect. 6.3.3).

Quantification is a persisting burden of LIBS analyses limiting its extensive use in real-life applications. The main drawback of quantitation in the case of tissues is the absence of matrix-matched standards. Their preparation from real-life samples is limited, while grounding and homogenization of the tissue and spiking it with selected analyte is contradictory to direct imaging of sectioned samples. Production of relevant reference samples is, thus, a subject of many research groups [70].

The case of hard tissues is rather straightforward when matrix-matched standards can be prepared directly from calcium carbonate, calcium oxalate, or hydroxyapatite. First, calcium carbonate was used for production of reference pellets spiked with traces of Al, Pb, and Sr to calibrate the quantitative LIBS analysis of juvenile teeth, adult teeth and bones [61]. Laser pulse energy, electron number density, and electron temperature were monitored during the experiment to ascertain fluctuations in signal feedback and to mitigate potential differences in physical properties between matrices of collected calcified tissues and artificial reference samples. Constructed

calibration curves for individual analytes (Al, Pb, and Sr) were internally standardized to the Ca line intensity and reached detection limits above ppm range (15, 95, and 30 ppm, respectively). Second, calcium oxalate was spiked with Cu, Mg, Sr, and Zn to provide reference standards in the analysis of human kidney stones while reaching tens to hundreds ppm detection level [71]. Third, hydroxyapatite reference samples were spiked with Co, Mn, Ni, Sr, and V prior the quantitative mapping of human teeth [72].

Soft tissues present a more intricate way of matrix-matched standards preparation. Various approaches of soft tissue preparation were utilized (e.g., homogenized pellets, inkjet solution printed on paper, gelatin gel) while the analyte content was administered through spiking [70]. The group of Motto-Ros produced a series of publications in which the quantification of Gd in murine kidneys was subjected. A rather controversial approach was used in their former study where solutions of Gd NPs were simply put on petri dishes and analyzed with the LIBS under the same conditions as soft tissues [26, 28]. More elaborate preparation followed when reference samples from EPON (1:1 mixture of diglycidyl ether and dodecenylsuccinic anhydride, density of 1.22 g/L) were spiked with dispersion containing Gd NPs [27, 29]. This approach provided matrix-matched standards and, in turn, enabled to quantify the content (up to 15 mM per spot) in the series of measurements monitoring the uptake and clearance of Gd NPs through murine kidneys.

The obstruction with matrix-matched standard preparation leads many researchers to utilize calibration-free approaches for quantification of LIBS data (CF-LIBS) [73]. The CF-LIBS demands the knowledge of plasma temperature which has to be accurately estimated for all elements present in the sample. Therefore, it is necessary to detect broader spectral ranges encompassing multiple spectral lines of individual elements to construct Boltzmann plot or even Saha-Boltzmann plot. CF-LIBS was used in the analysis of human hair and nails [74], and gallstones [75]. Most recently, CF-LIBS was used to quantitate Ba, Ca, Mg, and Sr in deer bones with a reasonable fluctuation reaching 10% [76].

6.3.2 Correlative Imaging

Elemental images of sample surfaces obtained through LIBS analysis are suitable for their comparison with other spectroscopic, microscopic, and even tomographic techniques. Such an approach is collectively called *correlative imaging* (also called *hyphenated* or *complementary analysis*) and attracted a great deal of attention in past years. In fact, the joint utilization of various techniques to yield complementary results is well described in several reviews elsewhere [12, 77]. The correlative imaging demands for a parallel processing of large data sets, which creates an increased computation burden. The recent progress is related to the advancement in data mining (including machine learning) providing more convenient ways of data handling and processing [78, 79].

As already stated, the combination of LIBS with LA-ICP-MS extends the performance capacity of both techniques when overshadowing drawbacks of one technique by advantages of another. This combination provides multi-elemental capability in its full sense, enabling the detection of major and macro-elements by LIBS and traces, as well as isotopes, by LA-ICP-MS. This approach was already used more than a decade ago for imaging Mg and Pb in sunflower plants [8], and Sr and Ca in prehistoric bear tooth [9]. It is worth mentioning that in those publications, the performance of LIBS and LA-ICP-MS was rather compared than complemented. A more recent work [10] showed the full potential of joint use of LIBS (C, H, K, O, and N) and LA-ICP-MS (Cu, Fe, P, Pt, and Zn) in an analysis of human tumor. Obtained images complemented the elemental information about the heterogeneity of the tumor and were compared with optical images of the tissues after hematoxylin and eosin (H/E) staining. The tandem use of LIBS and LA-ICP-MS is being optimized; however, their direct combination in one system is still obstructed with differing optimal ablation parameters of each technique. The combination of LIBS with XRF is, thus, more convenient while the non-destructive use of XRF may be used on the sample prior LIBS analysis [80]. It was shown that both techniques can be used in tandem complementing each other as well as cross-reference manner as demonstrated on the quantitation of Ca, Fe, K, Mn, P, and Si in a dried sugar cane leaf [81].

The combination of LIBS and Raman spectroscopy enables to provide complete chemical information (elemental and molecular, respectively). The main drawback is in the low repetition rate of Raman spectroscopy in general. The Raman signal is basically very weak with high fluorescence, thus longer expositions (~ 1 s) per spot are necessary. Methodological approaches are developed to overcome those limitations and in Raman spectroscopy the mapping and imaging approach must be differentiated [82]. In the point-by-point mapping, whole Raman spectra are detected in each spot showing various Raman shifts with respect to the investigated molecular bonds. On the other hand, Raman imaging provides a direct image of the selected Raman shift from the complete sample surface, but the other spectral information is lost. To the best of our knowledge, the LIBS and Raman techniques have not been used in the manner of correlative large-scale imaging of biological and other samples. However, it has to be mentioned that the joint use of LIBS and Raman was proved feasible and potentially beneficial, e.g., in the discrimination of algae [83] or bacteria [84].

The use of spectroscopic and tomographic techniques is a novel approach potentially providing complete information about the investigated sample. For those purposes, the use of LIBS and X-ray computed tomography (XCT) seems like a vital match. This combination has already been proved feasible in our recent publications [57, 85]. In our recent publication, LIBS and XCT were jointly used for the analysis of murine incisors [57]. Obtained results contributed to the finding of two distinct types of dentins: cementum versus enamel-facing dentin. The elemental analysis (with a focus on Ca and Mg) was extended with chemometrics, and hyperspectral images were processed through principal component analysis (PCA) and characteristic spectra were clustered through *k*-means clustering. XCT

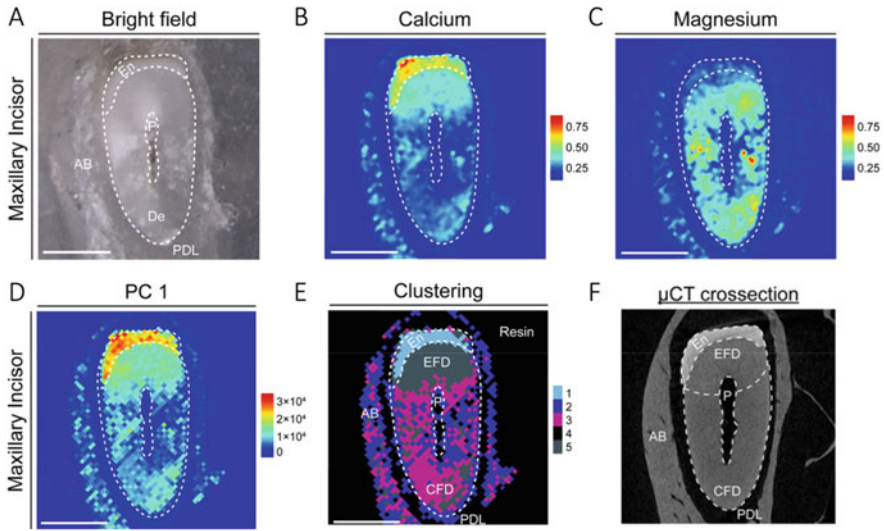


Fig. 6.6 (a–f) LIBS and XCT analysis of murine incisor. Obtained from [57] with permission and altered. Permission provided from John Wiley and Sons under contract number 5245561066199

volumetric data showed a change in the absorption coefficient in individual matrices/parts of the incisor (i.e., enamel, both dentins, and bone). The XCT image correlated with the LIBS elemental one and cluster images while setting a proof for the existence of two types of dentins (Fig. 6.6).

6.3.3 Multivariate Data Analysis for Imaging Purposes

Collected LIBS data carry characteristic information about investigated sample or relevant position on the sample, the so-called elemental fingerprint. As it was shown above, fine changes in spectral response of selected elemental lines can be related to unique differences between various tissues. However, understanding typical LIBS spectra is tedious namely for their high dimensionality and redundancy [79]. Chemometric and machine learning algorithms are becoming a standard in analytical chemistry [86], incl. LIBS data processing. Those algorithms improve the performance of clustering of characteristic spectra (e.g., related to healthy or diseased tissue) or even classification when the learning process is supervised. Machine learning algorithms were already implemented for the classification of various biological tissues. LIBS and Raman spectra of bacteria were joined together and clustered through Self-Organizing Maps (SOM) classifier after PCA dimensionality reduction [84]. LIBS spectra of deer bones were classified with the use of Artificial Neural Network (ANN) classifier [76]. It is noteworthy that PCA was combined with Linear Discriminant Analysis (LDA) to classify porcine samples (soft and hard tissues) [87].

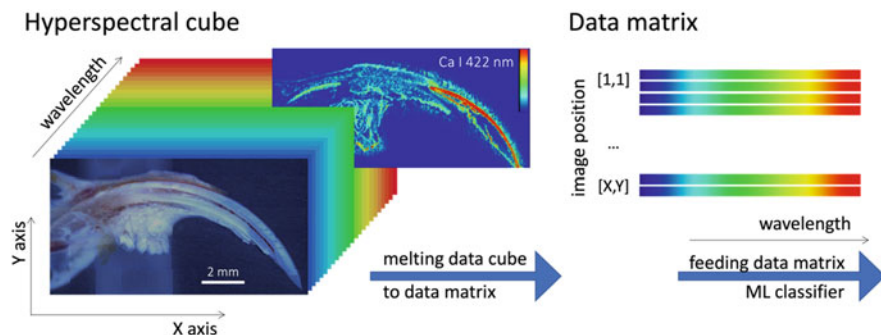


Fig. 6.7 Hyperspectral cube obtained from the analysis of the whole sample. Each $[X,Y]$ position is represented by a related LIBS spectrum. Each layer of high-dimensional data cube provides an elemental image on selected wavelength

The clustering/classification of soft tissue spectra has been repeatedly demonstrated; this is especially appealing in cancer research and other clinical applications. Many feasibility studies were delivered when discriminating healthy and cancerous tissues; e.g., Support Vector Machines (SVM) in the case of lung tumor [43]; LDA, SVM, and ANN were used for the identification of parathyroid gland [49]; SVM and Random Forrest (RF) algorithms were used to cluster brain tumor spectra [50].

The transition from point-by-point analysis to large-scale imaging results in the so-called hyperspectral data cube (Fig. 6.7). The data cube contains high-dimensional data that are organized into a data matrix (spectra as rows, wavelengths as columns) and assigned with metadata (e.g., x, y, and z positions). This simple data handling provides a data structure suitable for further application of machine learning algorithms and consequent clustering or classification of characteristic tissue spectra. The discrimination of melanoma and dermis spectra was proved feasible on mapping (200×200 spots with $15 \mu\text{m}$ steps) of murine skin tumors [47]. The wide spectral range (240–350, 340–450, and 720–800 nm) was downsized with the maximum likelihood technique and selected intensity ratios were then fed to an SVM classifier. Finally, to the best of our knowledge, our group was the first to deliver segmentation of hyperspectral cube (275–290, 380–405, 575–595, and 760–785 nm) obtained from the analysis of human cancer tissues (cutaneous cancers; such as malignant melanoma, basal cell carcinoma, and haemangioma) [46]. The data cube was processed with SOM classifier when showing regions of diseased tissues. Further research and optimization of machine learning (ML) algorithm is necessary in any of the selected publications. There is a clinical need for accurate differentiation of healthy and diseased tissues with highlighted boundary of cancer showing its proliferation throughout the tissue. Thus, this demands a fine-tuning of the ML model prediction and robust thresholding between characteristic spectral responses. However, understanding the performance of ML models is mandatory prior to any further step [78].

Since 2008, the Melikechi group has invested considerable efforts in data processing of LIBS analysis of various blood samples. In their first work [88], they provided a basic visualization of data (mice blood, organic compounds, and proteins) and their distinct separation in PCA space. After the initial success, more sophisticated studies were delivered; e.g., discrimination of healthy and ovarian cancer-prone mice through SVM of LIBS spectra [89]; classification of blood samples from healthy and melanoma-prone mice through LIBS and various classifiers (e.g., LDA, SVM) [90]. Then, Chen et al. analyzed human whole blood samples to guesstimate potential occurrence of cancer, lymphoma [91, 92].

6.4 Applications

Broad utilization of LIBS technique led to other bio-applications that are out of scope of this chapter. The investigation of medical samples is also related to the analysis of body fluids and liquids [3]. Considerable attention is also attracted by the potential utilization of LIBS in the detection, classification, and quantification of bacteria and other pathogens [93]. It is also worth mentioning that LIBS provides certain detection power in food analysis [94].

The use of LIBS in biological and medical/clinical applications has already been reviewed [3, 16–19, 65]. Thus, we aim to build on those reviews while offering another perspective to the discussion. Related bioimaging applications are concerned with the detection of elements, mostly metals, that are either naturally present in tissues (i.e., endogenous elements) or administered artificially to tissues (i.e., exogenous elements). In the following paragraphs, selected LIBS research is presented showing its capability to provide valuable information with sufficient sensitivity (reaching ppm level) and lateral resolution (10–100 μm).

6.4.1 Environmental and Plant Tissue Analysis

LIBS is also often used for environmental monitoring and analysis of plants [80, 95, 96]. As in the case of other bio-samples, the detection of macro and micro-nutrients was found to be important. Any change in their abundance within sample bulk (root, stem, leaf) can be correlated with the model-plant growth. There are numerous works that estimate the impact of fertilization and artificially induced stress (e.g., drought, nutrition deficiency, toxicity due to the presence of heavy metals and nanoparticles). Research is generally conducted in terms of qualitative comparison of characteristic spectra collected from various positions in plant organisms. Researchers showed that LIBS could contribute to the analysis of, e.g., wood preservatives [97], the impact of draught stress on gardenia and wheat [98], and Cr(VI) toxicity impact on wheat seedlings [99]. Moreover, quantification of macro-elemental concentration was also provided through chemometrics [100, 101]. The most recent work by Martin et al. [101] manifested the use of partial least squares regression (PLSR) for the determination of major elements (Ca, K, Mg, P, S, and Si) in switchgrass with an accuracy

reaching over 90%. LIBS results were compared to ICP-OES reference data and its capability for high-throughput analysis was recognized. Moreover, the combined use of LIBS and X-ray fluorescence (XRF) spectroscopy was proved beneficial for the determination of macro-elements (Ca, Fe, K, Mn, P, and Si) in dried sugar cane leaves [81]. Thus, LIBS has a clear potential to become a reliable technique for assessing feedstock quality (elemental composition) [96].

The laser ablation of plants shows a lower complexity in laser-plant interaction (due to the relatively hard matrix of plant tissues). Related LIBS experiments are relatively more straightforward in terms of sample preparation (samples grown in soil or in aqueous medium/hydroponic conditions) and handling (from grounding of dried plant to in-vivo analysis). The possibility to grow model samples with a high number of replicates is basically unlimited without any restrictions caused by ethical issues (as opposed to the case of animal and human samples). Despite all the listed advantages, the number of studies involved in large-scale imaging of plants with a high lateral resolution is considerably low [18, 19, 96]. Pioneering papers delivering the first mapping of plant tissues are dated to 2007. Kaiser et al. [102] studied hyperaccumulation of Pb and Cd within sunflower plants by using an fs LIBS. The plants were grown in hydroponic dispersion of various salts, which is typical for toxicology studies. Such an approach enables a fast growth of plants (within several days) with detectable content of toxic metals and a reasonable size of the whole plant (spread across the microscopic slide). In this study, LIBS was supported by X-ray radiography to provide high-resolution imaging of Pb and Cd within the plant leaves.

Since then, LIBS has proved to be an adequate tool for plant elemental imaging when showing the distribution of elements throughout the whole sample. Both in situ and in vitro analysis of plant tissues were demonstrated on maize leaves [59] via extension to 3D imaging. The body of work of Kaiser et al., reviewed among others in [19], significantly contributed to the development of LIBS as a complementary tool to standard plant toxicology. The development of micro-scale LIBS was manifested by Modlitbová et al. [103] when the performance of LIBS with 100 and 25 μm spot sizes was compared. Figure 6.8 illustrates the results used to elucidate the uptake, accumulation, and translocation of Cd-based quantum dots (Cd QDs) and Cd salts as a reference. The samples of white mustard were prepared in the short-term toxicity test (72 h) and were grown in a hydroponic dispersion.

A recent publication by Modlitbová et al. [58] presents LIBS as a straightforward tool for plant biologists which is capable to provide large-scale images. In this work, the typical pipeline of sample preparation and consequent analysis was shown in detail on cabbage. The model plant was grown in the hydroponic dispersion of Y-based upconversion nanoparticles (UCNPs) and Y salts as a toxic reference. Obtained results suggest the UCNPs to be relatively harmless to the model organism in low concentrations with root as the main storage organ and limited translocation to other parts of the plant (stem or leaf).

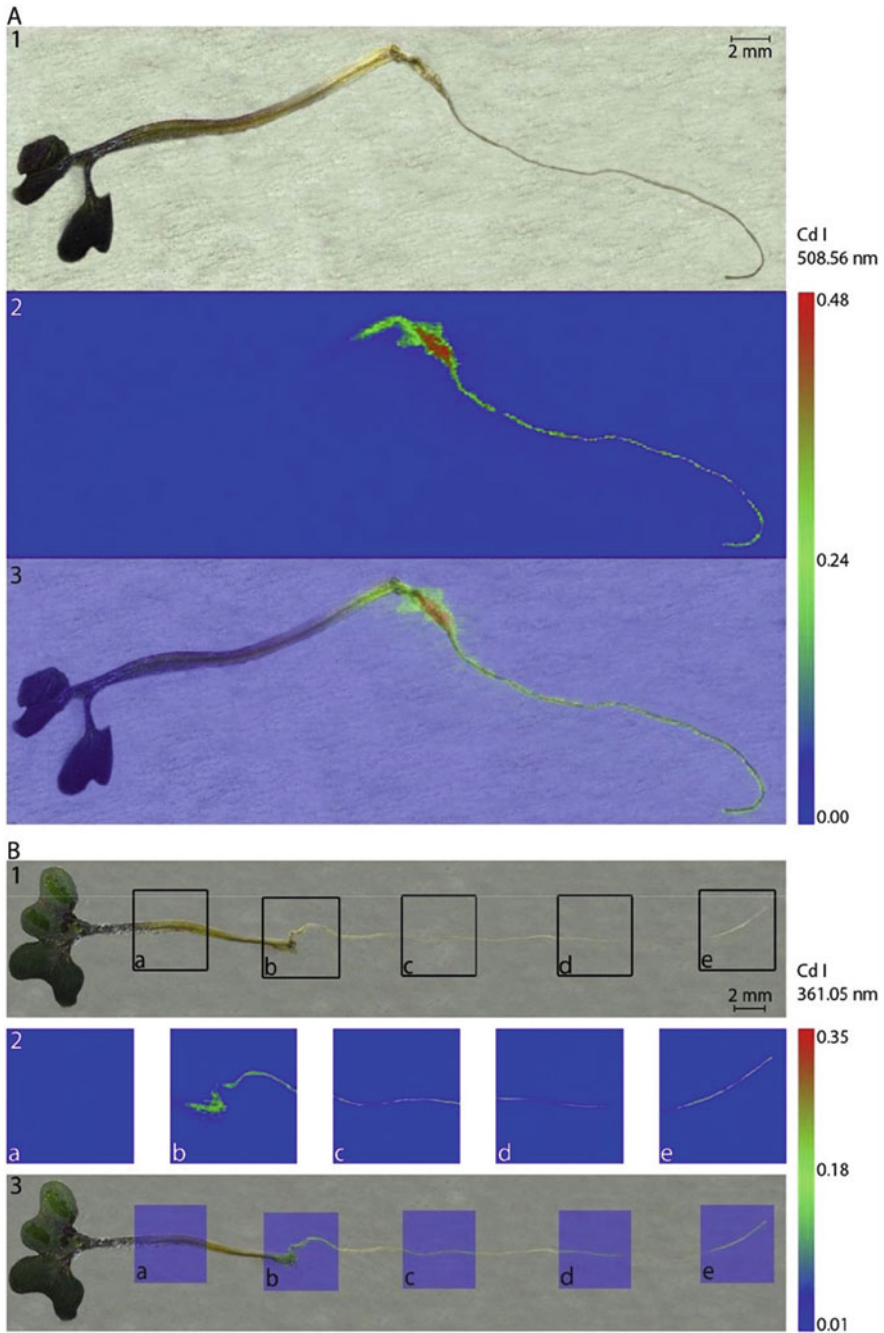


Fig. 6.8 (a) (1) Photograph of *S. alba* plant exposed to CdCl_2 at the nominal concentration $200 \mu\text{M}$ Cd before LIBS measurements. (2) LIBS maps constructed for Cd I 508.56 nm (3) Overlap of the original photograph of the plant with LIBS map. (b) (1) Photograph of *S. alba* plant exposed to CdCl_2 at the nominal concentration $200 \mu\text{M}$ Cd before micro-LIBS measurements together with

6.4.2 Bioimaging of Endogenous Elements

The bioimaging of endogenous elements can be considered as the direct detection (label-free) of biomarkers within investigated tissues. It was demonstrated that trace (e.g., Cu, Zn) and even macro elements (Ca, K, Mg, and Na) could be related with biological changes and diseases of tissues as they are manifested through the changes in chemical composition. Their essential presence and approaches to exploit changes in their abundance for the sake of various applications were already presented above.

The development of hard tissues is related to the calcification of soft tissues and formation of hydroxyapatite. The process of calcification is moderate in the presence of Mg. Thus, the presence of Ca, Mg, and P and their abundance is the most significant for any investigation of hard tissues. In our recent study, we have used LIBS for bioimaging of murine teeth (maxillary and mandibular incisors, and molars) [57]. In this work, LIBS was used among other techniques (incl. XCT) to uncover biological phenomena beyond the odontoblast development and led to a discovery of two distinct kinds of dentin tissues induced during the teeth growth of selected mice strains (DSPP-cerulean/DMP1-cherry) and mutants (Spry2^{+/-};Spry4^{-/-}). LIBS analysis contributed with fine elemental images (30 μm lateral resolution) of Ca and Mg. The finding of two dentin structures was supported by the use of PCA with *k*-means clustering showing two distinct clusters in the area of enamel and periodontal ligament.

Imaging of cancerous soft tissues revealed the importance of the detection of endogenous metals by LIBS. First, LIBS (C, H, K, Na, and O) was used in tandem with LA-ICP-MS (Cu, Fe, P, Pt, and Zn) to provide complementary bioimaging of human tumor tissues [10]. Second, various cancerous tissues were analyzed by LIBS to show distribution images of selected elements, e.g., Ca, Fe, Mg, Na, P, and Zn in malignant melanoma, Merkel cell carcinoma, and squamous cell carcinoma [35]; C and Mg in murine melanoma [38]; C, Ca, K, Mg lines and CN bands for discrimination of murine melanoma [47]; Al, Ca, Cu, Fe, Mg, Na, and Si for the estimation of lung cancer boundary [48]. Capability of 3D bioimaging was confirmed in the case of Ca, Cu, Mg, Na, and P in murine brain [45], and Ca, K, Mg, and Na in squamous cell carcinoma [46]. Our recent work [46] showed the capability of LIBS to image cutaneous cancer margins through direct imaging of biomarkers (namely Mg) as well as through SOM clustering. The increased content of Mg in the cancer region of malignant melanoma and basal cell carcinoma was in contrast with Mg deficiency in the region of benign hemangioma.

Fig. 6.8 (continued) marked spot analyzed by micro-LIBS (a,b,c,d,e); (2) Micro-LIBS maps constructed for the Cd I 361.05 nm line; (3) Overlap of the original photograph of the plant with micro-LIBS maps. The scale shows the total emissivity of the selected emission lines. Obtained from [103] with permission for reuse from Elsevier publishing under license number 5245750991187

6.4.3 Bioimaging of Exogenous Elements

The bioimaging of exogenous elements can be further divided into two main fields of interest. First, the study of the fate of artificially administered metallic NPs within an organism and the detection of foreign metals present in the organism due to environmental pollution or unhealthy lifestyle (e.g., smoking). Second, the detection of specifically bound nanoparticle labels in the frame of immunochemistry.

NPs are typically used as specific labels, contrasting agents, or drug carriers. Thus, monitoring their fate within the organism, accumulation in organs and natural clearance is of interest also to LIBS bioimaging. Motto-Ros introduced a series of publications with the focus on the detection of Gd-based NPs in murine kidneys [27–29] and with the extension to 3D bioimaging [33]. It was shown that NPs tend to accumulate in the outer part of kidney (cortex). Their clearance was monitored in several mice species over a week period. In another study, the accumulation of Au NPs and renal clearance was investigated through LIBS and synchrotron XCT [37]. The Au-based NPs first targeted the U87MG brain tumor in mice, as visualized in XCT volumetric data. Then, harvested organs (spleen, liver, and kidney) were imaged with LIBS. The use of LIBS for the detection of NPs as enhancers in radiation therapy was also demonstrated. Detappe et al. [32] showed the detection of silica-based gadolinium chelated nanoparticles in murine tumor. In recent studies, LIBS has been used for the detection of ^{10}B atoms in U87MG and U251MG brain tumors [40] and $\text{LaF}_3\text{:Ce}$ NPs in F98 brain tumor [41]. The aforementioned studies were delivered with a high lateral resolution reaching 10 μm . Further improvement is limited with standard ns laser sources, thus, fs laser was used to obtain the resolution below 1 μm in the imaging of InP NPs within cells [42]. Finally, it is worth mentioning that LIBS was used to detect Al, Cu, Ti, and W in various soft tissues (skin, lymph nodes, and lungs) [34]. The presence of those elements was of foreign origin (e.g., residual debris after surgery) and was relevant to the cases of individual patients.

LIBS essentially struggles with a trade-off between sensitivity and lateral resolution. However, reaching the cell-level resolution with sufficient sensitivity to trace metals is the main analytical challenge [18]. Various techniques are being developed to avoid the performance drawbacks of LIBS, e.g., characteristic labeling of tissues with nanoparticle tags for indirect detection of biomarkers [104]. The so-called Tag-LIBS was originally suggested by the group of Melikechi. They used two NP tags for indirect, yet specific detection of ovarian cancer (CA 125 marker) and leptin hormone in the basic multiplexing scheme [105]. Further works then exploited the advantages of Tag-LIBS; e.g., detection of CdTe quantum dots labeled metallothionein spread on polystyrene surface [106]; detection of streptavidin-coated Ag NPs as labels of human serum albumin [107]; detection of Au NPs as labels of *Escherichia coli* in lateral flow assay (no imaging) [108]. In our recent work, we have compared the performance of upconversion scanner and LIBS in the detection of HER2 biomarker of human breast cancer cells [104]. The Y-based upconversion NPs (UCNPs) showed an excellent specificity as tested on HER2-positive BT-474 cells and HER2-negative MDA-MB-231 cells. In general, LIBS

proved to be an adequate alternative to fluorescence and upconversion scanners for its comparable detection limits, higher dynamic range and no need for crafting of fluorescent-active labels.

6.5 Conclusion and Future Perspectives

As was repeatedly discussed in this chapter and highlighted in many publications, LIBS offers a vital alternative to other analytical techniques in the multi-elemental analysis of biological tissues on a large scale. It is primarily not intended to substitute other analytical techniques but to complement them and in turn to provide a more complete information about the investigated samples, to uncover the biological phenomena in their complexity. Thus, the tandem use of LIBS with LA-ICP-MS, Raman spectroscopy, or even XCT was found beneficial. However, the so-called correlative imaging most commonly relates LIBS elemental images with optical microscopy, e.g., images from histopathology.

A steady improvement of the LIBS instrumentation is aimed at its main benefits, i.e., high-throughput (above 100 Hz to units of kHz) and lateral resolution (below 10 μm). The analytical sensitivity is sacrificed for the sake of said benefits when the best possible detection limit is at the ppm level. Such sensitivity is sufficient for the detection of major and minor elements when also reaches traces for certain experimental parameters. This unique trade-off in analytical performance makes LIBS a potential prescreening tool for fast diagnostics of a higher number of samples.

Further improvement in sensitivity is expected with the constant improvement of utilized instrumentation (e.g., higher throughput of spectrometers, higher quantum efficiency of detectors). However, providing an accurate quantitative analysis is mandatory to strengthen the position of LIBS as a mature technique of analytical chemistry. So far, most of the research works have been concerned with qualitative or semi-quantitative analysis (i.e., showing relative change in the intensity on the sample surface). Production of matrix-matched standards is limiting the quantitation. Usual approaches match the chemical similarity, but not the physical matrix (physical properties, e.g., hardness). Recently, the lack of matrix-matched standards has been mitigated with the use of multivariate regression models and calibration-free algorithms.

LIBS is suitable for bioimaging of endogenous and exogenous elements in various applications, ranging from bioaccumulation of metals to medical/clinical use and immunochemistry. Despite the improvement of LIBS instrumentation, the number of publications presenting large-scale imaging of soft and hard tissues is rather low. The main limiting factors are advanced instrumentation control, tedious sample preparation and optimization of complex, mutually dependent parameters influencing laser-tissue interaction and consecutive laser ablation. Despite these, LIBS presented sufficient detection limits in the case of NPs which were beneficially used for enhancement of tumor radiotherapy and specific marking of selected proteins within tissue. The use of nanometallic labels makes LIBS a promising alternative to standard immunochemistry techniques.

LIBS bioimaging results in a large hyperspectral cube that carries multi-elemental information that can be related to individual spots on the sample surface. The simple projection of elemental maps over the sample surface is substituted with more sophisticated approaches. Advanced statistical algorithms are implemented to discriminate individual matrices of the sample (i.e., healthy and diseased tissues). Thus, future efforts will strive to deliver machine learning pipeline for a robust segmentation of elemental images which will significantly extend current state-of-the-art data processing in various applications (e.g., pathology, developmental biology).

Conclusions presented in reviewed literature sources are usually based on results of feasibility studies where only a small number of samples were analyzed. Such analyses uncover the potential of LIBS in various fields of interest; however, they are not fully convincing in terms of clinical use. It is therefore necessary to focus on analysis of series of samples to confirm causalities between significant chemical changes in tissues and related characteristic spectral response, i.e., cohort studies.

Acknowledgment The authors gratefully acknowledge the financial support of the Czech Science Foundation (GACR Standard, no. 22-27580S). PP and PM gratefully acknowledge the financial support of the Czech Science Foundation (GACR Junior, no. 20-19526Y).

References

1. Sabine Becker J. Imaging of metals in biological tissue by laser ablation inductively coupled plasma mass spectrometry (LA-ICP-MS): state of the art and future developments. *J Mass Spectrom.* 2013;48:255.
2. Jelínková H. Lasers for medical applications diagnostics, therapy and surgery. Cambridge: Woodhead Publishing; 2013.
3. Gaudiuso R, et al. Laser-induced breakdown spectroscopy for human and animal health: a review. *Spectrochim Acta B.* 2019;152:123.
4. Niemi MH. Laser-tissue interactions. Berlin: Springer; 2002.
5. Vogel A, Venugopalan V. Mechanisms of pulsed laser ablation of biological tissues. *Chem Rev.* 2003;103:577.
6. Kanawade R, et al. Qualitative tissue differentiation by analysing the intensity ratios of atomic emission lines using laser induced breakdown spectroscopy (LIBS): prospects for a feedback mechanism for surgical laser systems. *J Biophotonics.* 2015;8:153.
7. Mehari F, et al. Laser induced breakdown spectroscopy for bone and cartilage differentiation - ex vivo study as a prospect for a laser surgery feedback mechanism. *Biomed Opt Express.* 2014;5:4013.
8. Kaiser J, et al. Mapping of lead, magnesium and copper accumulation in plant tissues by laser-induced breakdown spectroscopy and laser-ablation inductively coupled plasma mass spectrometry. *Spectrochim Acta B.* 2009;64:67.
9. Galiová M, et al. Multielemental analysis of prehistoric animal teeth by laser-induced breakdown spectroscopy and laser ablation inductively coupled plasma mass spectrometry. *Appl Opt.* 2010a;49:C191.
10. Bonta M, Gonzalez JJ, Derrick Quarles C, Russo RE, Hegedus B, Limbeck A. Elemental mapping of biological samples by the combined use of LIBS and LA-ICP-MS. *J Anal At Spectrom.* 2016;31:252.
11. Becker JS, et al. Bioimaging of metals by laser ablation inductively coupled plasma mass spectrometry (LA-ICP-MS). *Mass Spectrom Rev.* 2010;29:156.

12. Doble PA, de Vega RG, Bishop DP, Hare DJ, Clases D. Laser ablation–inductively coupled plasma–mass spectrometry imaging in biology. *Chem Rev.* 2021;121:11769.
13. Francischini DS, Arruda MAZ. When a picture is worth a thousand words: Molecular and elemental imaging applied to environmental analysis – a review. *Microchem J.* 2021;169:106526.
14. Limbeck A, Galler P, Bonta M, Bauer G, Nischkauer W, Vanhaecke F. Recent advances in quantitative LA-ICP-MS analysis: challenges and solutions in the life sciences and environmental chemistry. *Anal Bioanal Chem.* 2015;407:6593.
15. Pozebon D, Scheffler GL, Dressler VL, Nunes MAG. Review of the applications of laser ablation inductively coupled plasma mass spectrometry (LA-ICP-MS) to the analysis of biological samples. *J Anal At Spectrom.* 2014;29:2204.
16. Busser B, Moncayo S, Coll JL, Sancey L, Motto-Ros V. Elemental imaging using laser-induced breakdown spectroscopy: a new and promising approach for biological and medical applications. *Coord Chem Rev.* 2018a;358:70.
17. Jolivet L, Leprince M, Moncayo S, Sorbier L, Lienemann CP, Motto-Ros V. Review of the recent advances and applications of LIBS-based imaging. *Spectrochim Acta B.* 2019;151:41.
18. Limbeck A, et al. Methodology and applications of elemental mapping by laser induced breakdown spectroscopy. *Anal Chim Acta.* 2021;1147:72.
19. Modlitbová P, Pořízka P, Kaiser J. Laser-induced breakdown spectroscopy as a promising tool in the elemental bioimaging of plant tissues. *Trends Anal Chem.* 2020a;122.
20. Carter S, Clough R, Fisher A, Gibson B, Russell B. Atomic spectrometry update: review of advances in the analysis of metals, chemicals and materials. *J Anal At Spectrom.* 2021;36:2241.
21. Galbács G. A critical review of recent progress in analytical laser-induced breakdown spectroscopy. *Anal Bioanal Chem.* 2015;407:7537.
22. Hahn DW, Omenetto N. Laser-induced breakdown spectroscopy (LIBS), part I: review of basic diagnostics and plasmaparticle interactions: still-challenging issues within the analytical plasma community. *Appl Spectrosc.* 2010;64:335.
23. Hahn DW, Omenetto N. Laser-induced breakdown spectroscopy (LIBS), part II: review of instrumental and methodological approaches to material analysis and applications to different fields. *Appl Spectrosc.* 2012;66:347.
24. Vanraes P, Bogaerts A. Laser-induced excitation mechanisms and phase transitions in spectrochemical analysis – Review of the fundamentals. *Spectrochim Acta B.* 2021;179:106091.
25. Motto-Ros V, et al. Mapping of native inorganic elements and injected nanoparticles in a biological organ with laser-induced plasma. *Appl Phys Lett.* 2012;101:223702.
26. Motto-Ros V, et al. Mapping nanoparticles injected into a biological tissue using laser-induced breakdown spectroscopy. *Spectrochim Acta B.* 2013;87:168.
27. Sancey L, et al. Laser spectrometry for multi-elemental imaging of biological tissues. *Sci Rep.* 2014a;4:1.
28. Sancey L, et al. Laser-induced breakdown spectroscopy: a new approach for nanoparticle's mapping and quantification in organ tissue. *J Vis Exp.* 2014b;88:1.
29. Sancey L, et al. Long-term in vivo clearance of gadolinium-based AGuIX nanoparticles and their biocompatibility after systemic injection. *ACS Nano.* 2015;9:2477.
30. Moussaron A, et al. Ultrasmall nanoplatforms as calcium-responsive contrast agents for magnetic resonance imaging. *Small.* 2015;11:4900.
31. Kunjachan S, et al. Nanoparticle mediated tumor vascular disruption: a novel strategy in radiation therapy. *Nano Lett.* 2015;15:7488.
32. Detappe A, et al. Advanced multimodal nanoparticles delay tumor progression with clinical radiation therapy. *J Control Release.* 2016;238:103.
33. Gimenez Y, et al. 3D imaging of nanoparticle distribution in biological tissue by laser-induced breakdown spectroscopy. *Sci Rep.* 2016;6:1.

34. Busser B, et al. Characterization of foreign materials in paraffin-embedded pathological specimens using in situ multi-elemental imaging with laser spectroscopy. *Mod Pathol.* 2018b;31:378.
35. Moncayo S, et al. Multi-elemental imaging of paraffin-embedded human samples by laser-induced breakdown spectroscopy. *Spectrochim Acta B.* 2017;133:40.
36. Török S, Limbeck A, Döme B, Bonta M. Tandem LA–LIBS coupled to ICP-MS for comprehensive analysis of tumor samples. *Spectroscopy.* 2017;32:42.
37. Le Guével X, et al. Elemental and optical imaging evaluation of zwitterionic gold nanoclusters in glioblastoma mouse models. *Nanoscale.* 2018;10:18657.
38. Moon Y, Han JH, Choi J, Shin S, Kim Y-C, Jeong S. Mapping of cutaneous melanoma by femtosecond laser-induced breakdown spectroscopy. *J Biomed Opt.* 2018;24:1.
39. Wei H, Zhao Z, Lin Q, Duan Y. Study on the molecular mechanisms against human breast cancer from insight of elemental distribution in tissue based on laser-induced breakdown spectroscopy (LIBS). *Biol Trace Elem Res.* 2021;199:1686.
40. Kalot G, et al. Aza-BODIPY: a new vector for enhanced theranostic boron neutron capture therapy applications. *Cell.* 2020;9:1953.
41. Bulin AL, et al. Radiation dose-enhancement is a potent radiotherapeutic effect of rare-earth composite nanoscintillators in preclinical models of glioblastoma. *Adv Sci.* 2020;7:1.
42. Meng Y, Gao C, Lin Z, Hang W, Huang B. Nanoscale laser-induced breakdown spectroscopy imaging reveals chemical distribution with subcellular resolution. *Nanoscale Adv.* 2020;2:3983.
43. Lin X, Sun H, Gao X, Xu YT, Wang ZX, Wang Y. Discrimination of lung tumor and boundary tissues based on laser-induced breakdown spectroscopy and machine learning. *Spectrochim. Acta Part B At Spectrosc.* 2021a;180:106200.
44. Šindelářová A, et al. Methodology for the implementation of internal standard to laser-induced breakdown spectroscopy analysis of soft tissues. *Sensors (Switzerland).* 2021;21:1.
45. Lin Q, Wang S, Duan Y, Tuchin VV. Ex vivo three-dimensional elemental imaging of mouse brain tissue block by laser-induced breakdown spectroscopy. *J Biophotonics.* 2021b;14:1.
46. Kiss K, et al. Imaging margins of skin tumors using laser-induced breakdown spectroscopy and machine learning. *J Anal At Spectrom.* 2021;32:909.
47. Choi JH, Shin S, Moon Y, Han JH, Hwang E, Jeong S. High spatial resolution imaging of melanoma tissue by femtosecond laser-induced breakdown spectroscopy. *Spectrochim Acta B.* 2021;179:106090.
48. Yin P, Hu B, Li Q, Duan Y, Lin Q. Imaging of tumor boundary based on multielements and molecular fragments heterogeneity in lung cancer. *IEEE Trans Instrum Meas.* 2021;70:1.
49. Wang Q, et al. Primary study of identification of parathyroid gland based on laser-induced breakdown spectroscopy. *Biomed Opt Express.* 2021;12:1999.
50. Teng G, et al. Predictive data clustering of laser-induced breakdown spectroscopy for brain tumor analysis. *Biomed Opt Express.* 2021;12:4438.
51. Buday J, Pořízka P, Kaiser J. Imaging laser-induced plasma under different laser irradiances. *Spectrochim Acta B.* 2020;168:105874.
52. Buday J, Pořízka P, Buchtová M, Kaiser J. Determination of initial expansion energy with shadowgraphy in laser-induced breakdown spectroscopy. *Spectrochim Acta B.* 2021;182:106254.
53. Jantzi SC, Motto-Ros V, Trichard F, Markushin Y, Melikechi N, De Giacomo A. Sample treatment and preparation for laser-induced breakdown spectroscopy. *Spectrochim Acta B.* 2016;115:52.
54. Bonta M, Török S, Hegedus B, Döme B, Limbeck A. A comparison of sample preparation strategies for biological tissues and subsequent trace element analysis using LA-ICP-MS. *Anal Bioanal Chem.* 2017;409:1805.
55. Moncayo S, et al. Exploration of megapixel hyperspectral LIBS images using principal component analysis. *J Anal At Spectrom.* 2018;33:210.

56. Mohamed N, et al. Chemical and mineralogical mapping of platinum-group element ore samples using laser-induced breakdown spectroscopy and micro-X-Ray fluorescence. *Geostand Geoanalytical Res.* 2021;45:539.
57. Lavicky J, et al. The development of dentin microstructure is controlled by the type of adjacent epithelium. *J Bone Miner Res.* 2022;37:323.
58. Modlitbová P, Střítežská S, Hlaváček A, Prochazka D, Pořízka P, Kaiser J. Laser-induced breakdown spectroscopy as a straightforward bioimaging tool for plant biologists; the case study for assessment of photon-upconversion nanoparticles in *Brassica oleracea* L. plant. *Ecotoxicol Environ Saf.* 2021;214:112113.
59. Zhao C, Dong D, Du X, Zheng W. In-field, in situ, and in vivo 3-dimensional elemental mapping for plant tissue and soil analysis using laser-induced breakdown spectroscopy. *Sensors (Switzerland).* 2016;16:1764.
60. Samek O, Beddows DCS, Telle HH, Morris GW, Liska M, Kaiser J. Quantitative analysis of trace metal accumulation in teeth using laser-induced breakdown spectroscopy. *Appl Phys A Mater Sci Process.* 1999;69:S179.
61. Samek O, et al. Quantitative laser-induced breakdown spectroscopy analysis of calcified tissue samples. *Spectrochim Acta B.* 2001a;56:865.
62. Samek O, Telle HH, Beddows DCS. Laser-induced breakdown spectroscopy: a tool for real-time, in vitro and in vivo identification of carious teeth. *BMC Oral Health.* 2001b;9:1–9.
63. Galiová M, et al. Investigation of the osteitis deformans phases in snake vertebrae by double-pulse laser-induced breakdown spectroscopy. *Anal Bioanal Chem.* 2010b;398:1095.
64. Dosedělová H, et al. Age-related changes in the tooth–bone interface area of acrodont dentition in the chameleon. *J Anat.* 2016;229:356.
65. Singh VK, Kumar V, Sharma J. Importance of laser-induced breakdown spectroscopy for hard tissues (bone, teeth) and other calcified tissue materials. *Lasers Med Sci.* 2015;30:1763.
66. Sasazawa S, Kakino S, Matsuura Y. Optical-fiber-based laser-induced breakdown spectroscopy for detection of early caries. *J Biomed Opt.* 2015;20:065002.
67. Kumar A, Yueh F-Y, Singh JP, Burgess S. Characterization of malignant tissue cells by laser-induced breakdown spectroscopy. *Appl Opt.* 2004;43:5399.
68. El-Hussein A, Kassem AK, Ismail H, Harith MA. Exploiting LIBS as a spectrochemical analytical technique in diagnosis of some types of human malignancies. *Talanta.* 2010;82:495.
69. Imam H, Mohamed R, Eldakroui AA. Primary study of the use of laser-induced plasma spectroscopy for the diagnosis of breast cancer. *Opt Photonics J.* 2012;02:193.
70. Martinez M, Baudelet M. Calibration strategies for elemental analysis of biological samples by LA-ICP-MS and LIBS – a review. *Anal Bioanal Chem.* 2020;412:27.
71. Singh VK, Rai AK, Rai PK, Jindal PK. Cross-sectional study of kidney stones by laser-induced breakdown spectroscopy. *Lasers Med Sci.* 2009;24:749.
72. Martinez M, Bayne C, Aiello D, Julian M, Gaume R, Baudelet M. Multi-elemental matrix-matched calcium hydroxyapatite reference materials for laser ablation: evaluation on teeth by laser-induced breakdown spectroscopy. *Spectrochim Acta B.* 2019;159:105650.
73. Legnaioli S, Campanella B, Pagnotta S, Poggialini F, Palleschi V. Self-calibrated methods for LIBS quantitative analysis. In: *Laser-induced breakdown spectroscopy.* Elsevier; 2020. p. 561–80.
74. Zhang S, et al. Quantitative analysis of mineral elements in hair and nails using calibration-free laser-induced breakdown spectroscopy. *Optik (Stuttg).* 2021;242:167067.
75. Singh VK, Singh V, Rai AK, Thakur SN, Rai PK, Singh JP. Quantitative analysis of gallstones using laser-induced breakdown spectroscopy. *Appl Opt.* 2008;47:G38.
76. Marín Roldán A, Dwivedi V, de los Terreros JYS, Veis P. Laser-induced breakdown spectroscopy (LIBS) for the analyses of faunal bones: assembling of individuals and elemental quantification. *Optik (Stuttg).* 2020;218:164992.
77. Kaiser J, et al. Trace elemental analysis by laser-induced breakdown spectroscopy - biological applications. *Surf Sci Rep.* 2012;67:233.

78. Képeš E, et al. Interpreting support vector machines applied in laser-induced breakdown spectroscopy. *Anal Chim Acta*. 2021;1192:339352.
79. Pořízka P, Klus J, Képeš E, Prochazka D, Hahn DW, Kaiser J. On the utilization of principal component analysis in laser-induced breakdown spectroscopy data analysis, a review. *Spectrochim Acta B*. 2018;148:65.
80. Arantes De Carvalho GG, et al. Recent advances in LIBS and XRF for the analysis of plants. *J Anal At Spectrom*. 2018;33:919.
81. Bueno Guerra MB, et al. Direct analysis of plant leaves by EDXRF and LIBS: microsampling strategies and cross-validation. *J Anal At Spectrom*. 2015;30:1646.
82. Gierlinger N, Schwanninger M. The potential of Raman microscopy and Raman imaging in plant research. *Spectroscopy*. 2007;21:69.
83. Pořízka P, et al. Application of laser-induced breakdown spectroscopy to the analysis of algal biomass for industrial biotechnology. *Spectrochim Acta B*. 2012;74–75:169–76.
84. Prochazka D, et al. Combination of laser-induced breakdown spectroscopy and Raman spectroscopy for multivariate classification of bacteria. *Spectrochim Acta B*. 2018a;139:6–12.
85. Prochazka D, et al. Joint utilization of double-pulse laser-induced breakdown spectroscopy and X-ray computed tomography for volumetric information of geological samples. *J Anal At Spectrom*. 2018b;33:1993–9.
86. Ayres LB, Gomez FJV, Linton JR, Silva MF, Garcia CD. Taking the leap between analytical chemistry and artificial intelligence: a tutorial review. *Anal Chim Acta*. 2021;1161:338403.
87. Rohde M, et al. The differentiation of oral soft- and hard tissues using laser induced breakdown spectroscopy – a prospect for tissue specific laser surgery. *J Biophotonics*. 2017;10: 1250.
88. Melikechi N, Ding H, Rock S, Marcano O. A, Connolly D. Laser-induced breakdown spectroscopy of whole blood and other liquid organic compounds. *Opt Diagnostics Sens VIII*. 2008;6863:686300.
89. Melikechi N, Markushin Y, Connolly DC, Lasue J, Ewusi-Annan E, Makrogiannis S. Age-specific discrimination of blood plasma samples of healthy and ovarian cancer prone mice using laser-induced breakdown spectroscopy. *Spectrochim Acta B*. 2016;123:33.
90. Gaudiuso R, et al. Using LIBS to diagnose melanoma in biomedical fluids deposited on solid substrates: limits of direct spectral analysis and capability of machine learning. *Spectrochim Acta B*. 2018;146:106.
91. Chen X, Li X, Yang S, Yu X, Liu A. Discrimination of lymphoma using laser-induced breakdown spectroscopy conducted on whole blood samples. *Biomed Opt Express*. 2018a;9: 1057.
92. Chen X, Li X, Yu X, Chen D, Liu A. Diagnosis of human malignancies using laser-induced breakdown spectroscopy in combination with chemometric methods. *Spectrochim Acta B*. 2018b;139:63.
93. Rehse SJ. A review of the use of laser-induced breakdown spectroscopy for bacterial classification, quantification, and identification. *Spectrochim Acta B*. 2019;154:50.
94. Sezer B, Bilge G, Boyaci IH. Capabilities and limitations of LIBS in food analysis. *Trends Anal Chem*. 2017;97:345.
95. Martin MZ, Labbe N, Wagner RJ. Application of high resolution laser-induced breakdown spectroscopy for environmental and biological samples. Berlin Heidelberg: Springer-Verlag; 2014.
96. Singh VK, et al. Review: application of LIBS to elemental analysis and mapping of plant samples. *At Spectrosc*. 2021;42:99.
97. Martin MZ, Labbé N, Riels TG, Wullschleger SD. Analysis of preservative-treated wood by multivariate analysis of laser-induced breakdown spectroscopy spectra. *Spectrochim Acta B*. 2005;60:1179.
98. Kunz JN, Voronine DV, Lee HWH, Sokolov AV, Scully MO. Rapid detection of drought stress in plants using femtosecond laser-induced breakdown spectroscopy. *Opt Express*. 2017;25:7251.

99. Tripathi DK, Singh VP, Prasad SM, Chauhan DK, Kishore Dubey N, Rai AK. Silicon-mediated alleviation of Cr(VI) toxicity in wheat seedlings as evidenced by chlorophyll fluorescence, laser induced breakdown spectroscopy and anatomical changes. *Ecotoxicol Environ Saf.* 2015;113:133.
100. Martin MZ, et al. Correlating laser-induced breakdown spectroscopy with neutron activation analysis to determine the elemental concentration in the ionome of the *Populus trichocarpa* leaf. *Spectrochim Acta B.* 2017;138:46.
101. Martin M, Brice D, Martin S, André N, Labbé N. Inorganic characterization of switchgrass biomass using laser-induced breakdown spectroscopy. *Spectrochim Acta B.* 2021;186:106323.
102. Kaiser J, et al. Monitoring of the heavy-metal hyperaccumulation in vegetal tissues by X-ray radiography and by femto-second laser induced breakdown spectroscopy. *Microsc Res Tech.* 2007;70:147.
103. Modlitbová P, et al. Detail investigation of toxicity, bioaccumulation, and translocation of Cd-based quantum dots and Cd salt in white mustard. *Chemosphere.* 2020b;251:126174.
104. Pořízka P, et al. Laser-induced breakdown spectroscopy as a readout method for immunocytochemistry with upconversion nanoparticles. *Microchim Acta.* 2021;188:1.
105. Markushin Y, Melikechi N. Sensitive detection of epithelial ovarian cancer biomarkers using tag-laser induced breakdown spectroscopy. *Ovarian Cancer Basic Sci Perspect.* 2012; 17:153–70.
106. Konecna M, et al. Identification of quantum dots labeled metallothionein by fast scanning laser-induced breakdown spectroscopy. *Spectrochim Acta B.* 2014;101:220.
107. Modlitbová P, et al. Laser-induced breakdown spectroscopy as a novel readout method for nanoparticle-based immunoassays. *Microchim Acta.* 2019;186:1.
108. Gondhalekar C, et al. Detection of *E. coli* labeled with metal-conjugated antibodies using lateral-flow assay and laser-induced breakdown spectroscopy. *Anal Bioanal Chem.* 2020;412:1291.